



## City Research Online

### City, University of London Institutional Repository

---

**Citation:** Alali, A. A. & Tsavdaridis, K. (2024). Experimental Investigation on Flexural Behaviour of Prefabricated Ultra-Shallow Steel Concrete Composite Slabs. *Journal of Constructional Steel Research*, 217, 108632. doi: 10.1016/j.jcsr.2024.108632

This is the published version of the paper.

This version of the publication may differ from the final published version.

---

**Permanent repository link:** <https://openaccess.city.ac.uk/id/eprint/32571/>

**Link to published version:** <https://doi.org/10.1016/j.jcsr.2024.108632>

**Copyright:** City Research Online aims to make research outputs of City, University of London available to a wider audience. Copyright and Moral Rights remain with the author(s) and/or copyright holders. URLs from City Research Online may be freely distributed and linked to.

**Reuse:** Copies of full items can be used for personal research or study, educational, or not-for-profit purposes without prior permission or charge. Provided that the authors, title and full bibliographic details are credited, a hyperlink and/or URL is given for the original metadata page and the content is not changed in any way.

---

---

---

City Research Online:

<http://openaccess.city.ac.uk/>

[publications@city.ac.uk](mailto:publications@city.ac.uk)

---



# Experimental investigation on flexural behaviour of prefabricated ultra-shallow steel concrete composite slabs

Ahmed Abdulla Alali<sup>a,b</sup>, Konstantinos Daniel Tsavdaridis<sup>c,\*</sup>

<sup>a</sup> School of Civil Engineering, Faculty of Engineering and Physical Sciences, University of Leeds, Woodhouse Lane, LS2 9JT Leeds, UK

<sup>b</sup> Department of Civil Engineering, College of Engineering, University of Bahrain, Isa Town 32038, Kingdom of Bahrain

<sup>c</sup> Department of Engineering, School of Science & Technology, City, University of London, Northampton Square, EC1V 0HB London, UK

## ARTICLE INFO

### Keywords:

Flexural tests  
Composite slabs  
Ultra-shallow flooring system  
Lightweight concrete  
Shear connectors  
Shear studs

## ABSTRACT

This paper presents the test results of four static full-size four-point bending tests to investigate the flexural behaviour of a recently developed prefabricated steel-concrete composite ultra-shallow flooring system (PUSS®). The flooring system comprises of T-ribbed concrete floors partially-embedded within and connected to side C-channel beams and horizontally-oriented shear connectors. This study investigates the effects of three parameters on the flexural behaviour of PUSS® and the performance of the shear connectors under bending. The parameters under study are the type of concrete, degree of shear connection and depth of the slab. Four 4 m span test specimens are constructed using two types of concrete, two with reinforced normal weight concrete (NWC) and the remaining two with reinforced lightweight aggregates concrete (LWC). Three of the test specimens employ the unique shear connection system composed of horizontally-oriented steel dowels with horizontally-oriented web-welded shear studs (dowels with WWSS) while the last one employs horizontal steel dowels only. The contribution of the above parameters on flexural behaviour and failure mechanisms are examined. The study concludes that replacing NWC with LWC of similar strength does not affect the flexural behaviour of PUSS® in terms of slab capacity, ductility and failure mechanism. However, LWC demonstrates lower initial stiffness and leads to the development of larger cracks as loads increases. Also, reducing the degree of shear connection lowers the moment capacity of the slabs and results in failure of some shear connectors during testing. PUSS® units exhibit ductile behaviour under bending conditions regardless of the degree of shear connection.

## 1. Introduction

Steel-Concrete Composite (SCC) structural systems are integral to the advancement of the construction industry and have garnered significant research attention due to their efficiency in material utilisation, cost reduction and ability to provide high strength. SCC involves the combination of steel and concrete into a unified component, creating composite action between the two materials. The integration results in a singular, high-performance entity that surpasses the capabilities achieved by individual materials.

SCC flooring systems represent one of the widespread SCC structural elements, and their evolution over the past decades has contributed to enhancing the quality of the floorings in buildings, the increase of spans, the mitigation of vibrations and the material reduction. This progression commenced with traditional downstand steel beams where concrete slabs positioned on top of the steel beams flange to form a composite

beam. Subsequently, developments led to the integration of the slab thickness within the depth of the steel beam forming optimised composite slim floors [1]. Various slim floor systems have been developed over the years, including slim-floor constructed with deep composite decking, slim-floor constructed with precast concrete slab, ultra-shallow floor beams (USFB) and composite slim-floor beams (CoSFB). These systems share a common advantage of connecting concrete slabs to the steel beams within their structural depth, resulting in a reduced overall depth of the flooring system and thus the overall height of the building. In addition, these systems offer quick construction by using less or no propping and providing large uninterrupted floor areas. This enhances the building's flexibility capacity. As a result, such kind of systems are widely used and gained popularity in the construction sector. However, it has been observed that to achieve spans longer than 10 m, these systems require depths exceeding 300 mm to increase the bending resistance of the slab, even when lightweight concrete is used. The

\* Corresponding author.

E-mail address: [konstantinos.tsavdaridis@city.ac.uk](mailto:konstantinos.tsavdaridis@city.ac.uk) (K.D. Tsavdaridis).

<https://doi.org/10.1016/j.jcsr.2024.108632>

Received 25 September 2023; Received in revised form 19 March 2024; Accepted 23 March 2024

Available online 3 April 2024

0143-974X/© 2024 The Authors. Published by Elsevier Ltd. This is an open access article under the CC BY license (<http://creativecommons.org/licenses/by/4.0/>).

increased depth leads to higher material consumption, increased weight, and the possibility of shear failure. Consequently, there is a need for further improvements to steel-concrete composite flooring systems to make them more economically viable [2–4].

Over the previous decade, considerable attention has been directed towards the performance of the shear connectors in these slim flooring systems capitalising on the connection between the steel and the concrete to control stiffness, strength, and ductility. Several innovative shear connection systems have been introduced and studied while many of them demonstrated favourable outcomes and promising results. Among the trends in the advancement of the shear connectors of slim floors, the utilisation of horizontally oriented shear connectors has gained prominence, moving away from the traditional vertical shear studs. Several types of horizontal shear connectors have been examined in the literature, such as web-welded shear studs, concrete dowels (through web openings) and concrete dowels with steel tie bars (dowels) [5,6]. The primary research focus has been on the performance of such shear connectors in slim composite beams, loading them experimentally and numerically to direct shear [3,7–10] and flexural loading tests [3,11–14].

Moreover, the sustainability of structural elements is a crucial consideration that needs to be examined before selecting the appropriate structural system for a project. In the context of residential and office buildings, especially tall ones, floors constitute a significant proportion of the total weight (load) and material consumption, resulting in high environmental impacts (carbon footprint). Studies demonstrated that buildings account for approximately 40% of the global material flow, with the cement industry alone responsible for about 7% of the worldwide CO<sub>2</sub> emissions [15,16]. On-site construction is a considerable source of material waste and carbon emissions, primarily from fuel consumption during material transportation and the operation of heavy equipment. Conversely, off-site prefabrication enhances quality control and site safety, and reduces material waste, adverse environmental impacts, labour work, and construction time, which makes it a sustainable construction practice [17]. Therefore, innovative designs that facilitate the use of less and lighter materials can significantly contribute to carbon reduction and align with sustainability objectives.

## 2. PUSS® flooring system

This paper focuses on studying a recently developed and patented (WO2023139385A1 WIPO (PCT)) ultra-shallow flooring system known as Prefabricated Ultra-Shallow Slab (PUSS®). This innovative flooring system was initially developed in 2017 and research revealed its quick and efficient production capabilities and its potential to develop sustainable lightweight and high-strength slim floor systems. According to BS EN 1992-1-1 [18] and SCI P359 [19], the limiting span/depth ratio for single span slabs is 20. The significance of shallow floors appears in their ability to achieve higher span/depth ratios, saving both construction materials and overall cost. The unique configuration and the synergy of the working materials of PUSS® flooring system minimises its structural depth, resulting in ultra-shallow floors, which exhibit a shallower depth (greater span/depth ratio) compared to other existing shallow flooring systems, such as RC, Cofradal, and hollow core precast flooring systems. For instance, in case of the 230 mm deep PUSS® units investigated in the experiments, the single span slab can reach about 8 m span without the need for a finishing layer, providing span/depth ratio value exceeding 34, which is higher than the ratios that can be reached by the previously mentioned flooring systems and of similar ratios to the state-of-art CoSFB.

The standard version of a PUSS® system features a 230 mm depth and a large unit width of 2 m (reducing the number of erection lifts while meeting the transportation requirements). Units are fabricated by casting in-place reinforced ribbed concrete slabs within two parallel flange PFC C-channel steel beams, which are connected with one of three novel shear connection systems. These systems consist of either (1)

horizontally-oriented web-welded shear studs (WWSS), (2) horizontal steel dowels welded to the webs, or (3) a combination of both shear connection systems (WWSS with dowels) [20]. The horizontal steel dowels connections pass through the through the slab from one edge steel beam to the other, which makes them useful during the process of casting concrete as they hold the two edge beams in place, minimising the need for additional framework. PUSS® units are constructed off-site, performing all the necessary steel fabrication and welding processes first, then, ribbed concrete slabs are casted in-place utilising the steel edge beams as part of the concrete mould. After curing, the pre-fabricated slabs are moved as ready-made floor units to the construction site and installed at their intended locations in the building. Fig. 1 shows a schematic representation of a 1.6 m long segment of a standard PUSS® unit featuring a connection system composed of a combination of WWSS and steel dowels. Fig. 2 displays a grid of PUSS® flooring system composed of five PUSS® units supported by beams by sitting on their bottom flange and within their depth. A typical downstand beam arrangement with the PUSS® units on top, can also be configured.

Previous studies of PUSS® have emphasised its advantages, highlighting its light weight, which is a result of the use of lightweight concrete along with troughs and ribs running below the thin concrete flange between the two-side steel C-channel beams while providing an effective shear connection system within. That facilitates the construction of lightweight buildings, as slabs contribute significantly to the overall weight of the structures. In addition, the slabs' shape, characterised by regular voids underneath the ribbed slab permits the integration of building services and ceiling fixtures, thereby reducing the overall building height [20]. Moreover, the design accommodates the placement of acoustic insulation materials within the depth of the slab.

Furthermore, the outcomes of the previous Life Cycle Assessment (LCA) and Life Cycle Cost (LCC) studies conducted on the flooring

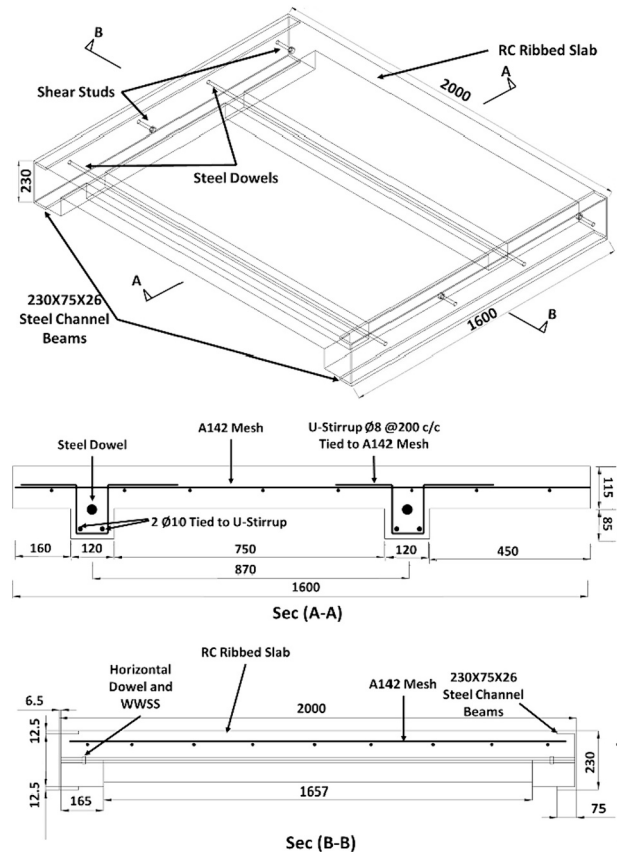


Fig. 1. Schematic drawing of a 1.6 m segment of a standard PUSS® flooring unit with steel dowel and WWSS shear connection system [21].

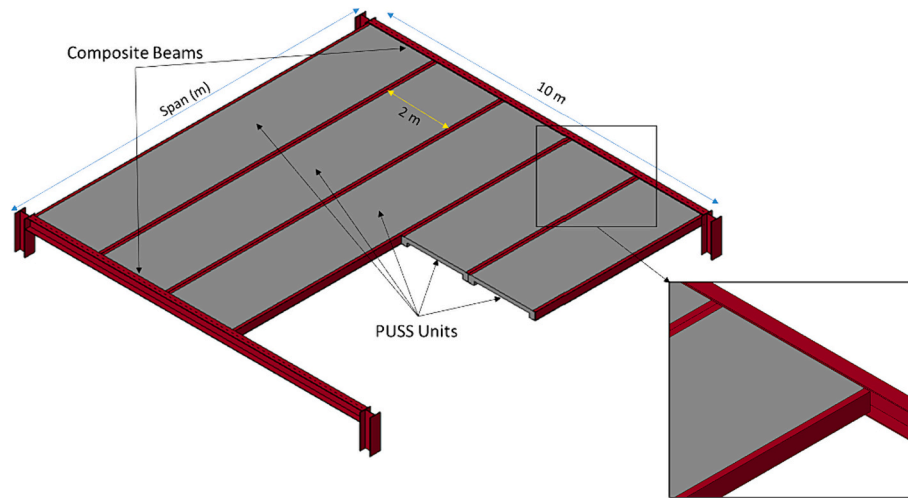


Fig. 2. Grid of PUSS® Flooring System.

system demonstrated numerous advantages in comparison to the widely used hollow core precast (HCU) slabs and the Cofradal slabs. The LCA indicated a considerable decrease in the overall Global Warming Potential (GWP), energy consumption, time and cost in comparison to the two aforementioned prefabricated slab systems. Moreover, the implementation of wider units made of lightweight materials reduces the number of necessary lifts during slabs installation, consequently lowering the overall transportation cost, construction time and energy consumption. Another benefit is the overall decrease in the CO<sub>2</sub> emissions and energy consumption starting from the materials extraction stage to the end-of-life (EoL) stage. In addition, the well-monitored and controlled prefabrication offsite significantly reduces the required onsite work, which usually causes construction errors and tends to be more costly compared to offsite work [22].

The performance of two shear connection systems employed in the proposed flooring system, namely, the horizontally oriented WWSS system and the horizontal dowels with WWSS system, were previously subjected to experimental investigation under direct static shear force using the push-out test methodology. Furthermore, numerical investigations were carried out through a finite element parametric study of PUSS® slabs. The investigations tested three distinct concrete types: normal weight concrete (NWC), lightweight aggregate concrete containing Lytag aggregates (LWC), and ultra-lightweight aggregate concrete containing Leca aggregates made of expanded clay (ULWC). The observations of the research indicated that the implementation of a combination of WWSS with dowels leads to higher shear capacities in comparison to WWSS alone. This is because steel dowels provide larger bearing area with concrete as they pass through the slabs from one edge to the other, which results in increasing the maximum shear resistance of the shear connection system. As a result of the research, a formula was developed to calculate the shear resistance of the shear connection systems (Eq. 1). Through comparison to both experimental and FEA outcomes, this equation showed a great match of the calculated shear resistances of shear connectors, varying in diameter from 16 mm to 22 mm, and assessed across PUSS® units utilising NWC, LWC or ULWC, with strengths ranging from 16 MPa and 30 MPa [9].

$$P_{sd} = 1.873(f_{ck}da_r)^{0.835} \leq 0.8f_uA_s \quad (1)$$

Where:  $P_{sd}$  is the shear resistance of shear stud or dowel.

$f_{ck}$  is the cylinder compressive strength of concrete.

$d$  is the diameter of stud or dowel.

$a_r$  is the distance from first stud or dowel to the top of concrete.

$f_u$  is the ultimate tensile strength of the material of the stud or dowel which should not be  $>500 \text{ N/mm}^2$ .

$A_s$  is the cross-sectional area of the shear stud or dowel.

In this study, the tests/FEA results showed better agreement with the derived equation in comparison to the shear capacity equations available in the design codes. The design codes used for comparison are Annex C of Eurocode 4 [23] (Eq. 2) which evaluates the shear strength of the horizontal lying shear stud connectors responsible for splitting of concrete in the direction of slab thickness, ANSI/AISC 360–10 [24] (Eq. 3) and AASHTO [25] (Eq. 4).

$$P_s = 1.4k_v(f_{ck}da_r')^{0.4} \left(\frac{a}{s}\right)^{0.3} / \gamma_v \leq 0.8f_u\pi d^2 / \gamma_v \quad (2)$$

Where:  $P_s$  is the shear resistance of shear stud.

$k_v = 1$  for shear connection in an edge position and 1.14 for a middle position.

$a_r'$  is the effective edge distance  $\geq 50 \text{ mm}$ .

$a$  is the horizontal spacing of studs with  $110 \leq a \leq 440 \text{ mm}$ .

$s$  is the spacing of stirrups with both  $a/2 \leq s \leq a$  and  $s/a_r' \leq 3$ .

$\gamma_v$  is a partial factor = 1.25

$$P_s = 0.5A_s\sqrt{f_{ck}E_c} \leq 0.75f_uA_s \quad (3)$$

Where:  $E_c$  is the modulus of elasticity of concrete.

$$P_s = \phi 0.5A_s\sqrt{f_{ck}E_c} \leq 0.75f_uA_s \quad (4)$$

Where:  $\phi$  is the resistance factor for the shear connectors = 0.85.

Comparing the three equations above shows that Eq. 3 and Eq. 4 take the effect of the lightweight concrete on the shear resistance of the shear connectors by including the modulus of elasticity of concrete in the equations. However, there is no consideration of this effect in Eq. 2. Therefore, the modification factor  $\lambda$  which is suggested by ACI 318 [26] to have the value of 0.75 for lightweight aggregates concrete is added to the calculations made using Eq. 2.

### 3. Experimental investigation

The details of four 4-point bending test specimens and test procedures conducted in this study are presented in the following sections.

#### 3.1. Details of test specimens

In the construction practices, PUSS® slabs are designed to have a fixed width of 2 m. This dimension is selected taking into consideration the possibility to fit in transportation means [20]. However, for the flexural tests, PUSS® specimens were scaled down to fit the restrictions

on the available lab space. The designed specimens were kept within practical dimensions with 4.4 m length (4 m clear span) and 1.1 m width, which represent scaled down models of true slabs with 7.3 m spans. The tests investigate the effects of:

- 1) Two shear connection systems:
  - a. WWSS with dowels
  - b. Dowels only
- 2) Two types of concrete:
  - a. Normal weight concrete
  - b. Lightweight aggregates concrete using Lytag aggregate
- 3) Two steel sections (with different depths):
  - a. 230 mm depth (steel section 230x75x26 PFC C-channel)
  - b. 300 mm depth (steel section 300x100x46 PFC C-channel)

Two 230x75x26 PFC C-channel steel sections are used as edge beams for three specimens, while two 300x100x46 PFC C-channel steel sections are used for specimen NWC-300-SD. For the three of the specimens, the shear connection system is composed of three steel dowels of  $\varnothing 20$  mm (spanning across the width) welded to the web posts of each PFC C-channel passing through the slabs ribs. In addition, two shear studs with  $\varnothing 16$ mm are welded horizontally to the web posts of each beam at the remaining two rib locations, as shown in Fig. 3. For LWC-230-D specimen, only three steel dowels with  $\varnothing 20$  mm are used. Note that for all the tested specimens, shear connectors are welded at the midpoint of the slab depth, at a depth of 115 mm for specimens with 230 mm depth, and at a depth of 150 mm for the fourth specimen, which has 300 mm depth. Finally, two of the specimens are cast with normal weight concrete and the other two with lightweight concrete – with Lytag aggregates. Fig. 4 illustrates the transverse and longitudinal cross sections details of test specimens with 230 mm depth. In addition, the dimensions and differences between the test specimens are presented in Table 1.

The implemented shear connectors, which are a combination of

WWSS and steel dowels or steel dowels only, compose the longitudinal shear connection system. However, the longitudinal shear connection system also affects the bending resistance of PUSS® units due the composite action between steel beams and the concrete slab. Using the principle of equilibrium between tension and compression, the depth of plastic neutral axis (P.N.A.) in PUSS® units can be calculated at different degrees of shear connection, where the degree of shear connection  $\eta$  ( $\eta = R_q/R_c$ ) is the ratio of the longitudinal shear resistance of the shear connectors,  $R_q$  to the compressive resistance of the slab in full shear connection,  $R_c$ .

In order to estimate the required type, spacing and size of shear connectors to achieve full shear connection in the first two specimens, and to evaluate the degree of shear connection ( $\eta$ ) in the remaining specimens, the shear resistance of the employed shear connectors and the longitudinal shear between steel beams and concrete slab need to be evaluated. Eq. 1 is utilised in this study to assess the shear resistance of the shear connectors. However, it is important to note that the procedure outlined in Eurocode 4 [27] for calculating longitudinal shear between steel and concrete is not directly applicable to the studied flooring system. This procedure is primarily designed for vertical headed shear studs connecting top concrete slabs to bottom steel beams. In the case of PUSS® units, horizontal shear connectors welded to the sides of the steel beams connect them to the concrete slab. Therefore, an alternative approach is adopted in this study to evaluate the longitudinal shear between steel and concrete, which is based on the concept of shear flow in built-up members ( $q$ ).

$$q = VQ/I \quad (5)$$

Where:  $q$  is the shear flow between the composite members (steel section and concrete) in unit of shear force per unit of length.

$V$  is the value of the shear force at the section.

$Q$  is the first moment of area of steel section in relation to the neutral axis.

$I$  is the moment of inertia of the entire cross-section about the neutral axis.

The calculation of shear flow of each specimen involves substituting the shear force related to the section's bending moment capacity. Then, the total longitudinal shear force between steel and concrete is determined by multiplying the shear flow ( $q$ ) by the shear span. Finally, the necessary spacing and size of shear connectors to achieve full shear connection are estimated using their shear resistance capacities derived from Eq. 1. It is worth noting that the calculated total longitudinal shear forces between steel side beams and concrete slab are relatively small and the utilisation of only 5 shear connectors with 870 mm spacing on each side of the slabs of 230 mm depth is sufficient to achieve full degree of shear connection. This is primarily due to the relatively low magnitude of first moment of area associated with steel sections ( $Q$ ) as they are small in area their neutral axes are close to the neutral axes of the composite sections.

### 3.2. Specimens preparation and materials properties

The fabrication of formwork and shuttering for the concrete ribbed slabs and steelwork (from welding of shear connectors to shaping of reinforcements) were conducted by SC4 Ltd. (a British steel fabricator). In addition, to provide lifting anchors for the slabs, holes with 50 mm diameter were drilled at the two ends of the side C-channel steel beams. Ready-mix concretes conforming to BS EN 197-1 [28] were cast in the prepared formworks at the worksite of SC4 and a vibrator was used to ensure appropriate compaction (Fig. 5).

NWC and LWC used in the four specimens were both of concrete class 20/25, with a maximum aggregate size of 14 mm. Slump tests on both types of concrete gave an average of around 100 mm slump (Fig. 6). From the concrete cubes and cylinders samples taken from the cast concrete, the density of NWC and LWC were measured to be 2230 kg/m<sup>3</sup>

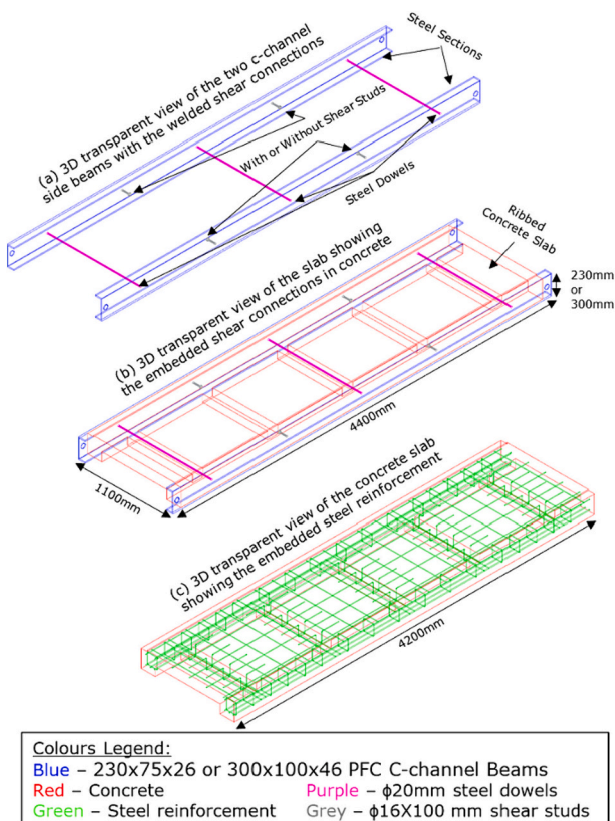


Fig. 3. 3D view of the details of test specimens.

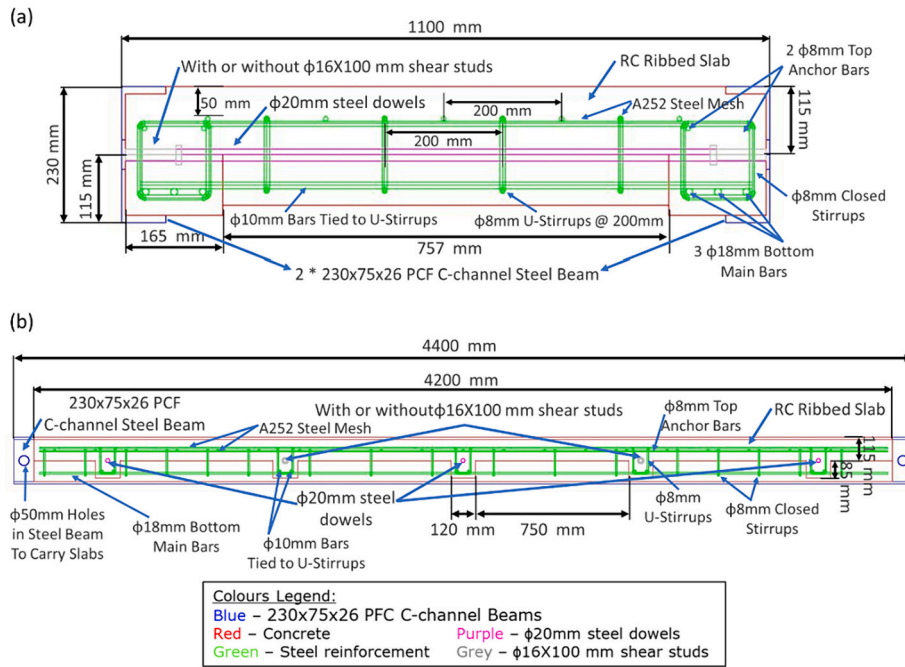


Fig. 4. (a) Transverse and (b) longitudinal cross sections details of specimens with 230 mm depth.

Table 1  
Specimen test matrix.

Specimen #	Specimen name	Width	Length	Depth	Steel beam size	Concrete type	Shear connectors	Degree of shear connection ( $\eta$ )
1	NWC-230-SD	1.1 m	4.4 m	230 mm	230x75x26	NWC*	3 x 20mm $\varnothing$ steel dowels with	100%
2	LWC-230-SD				PFC C-channel	LWC*	4 x 16mm $\varnothing$ WWSS	100%
3	LWC-230-D		4 m span			LWC	3 x 20mm $\varnothing$ steel dowels only	67%
4	NWC-300-SD			300 mm	300x100x46	NWC	3 x 20mm $\varnothing$ steel dowels with	57%
					PFC C-channel		4 x 16mm $\varnothing$ WWSS	

\*NWC and LWC stand for normal weight concrete and lightweight concrete with Lytag, respectively.

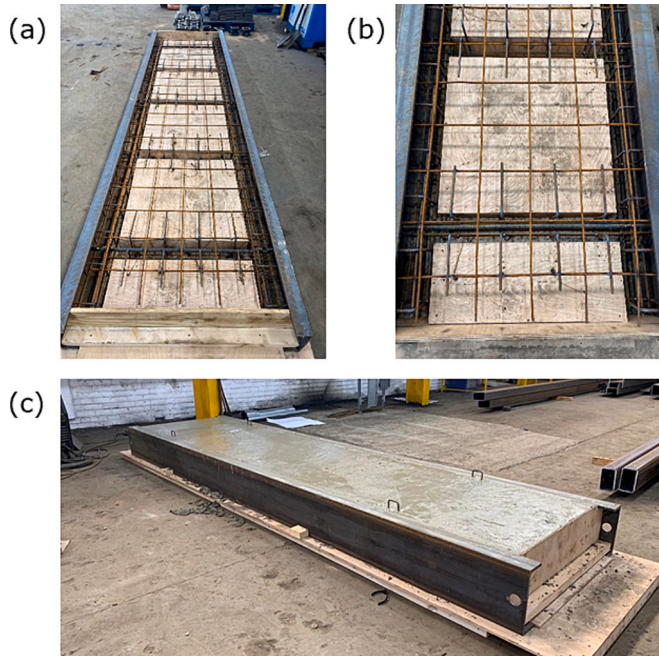


Fig. 5. (a), (b) Prepared specimens before casting concrete (c) Cast specimen.

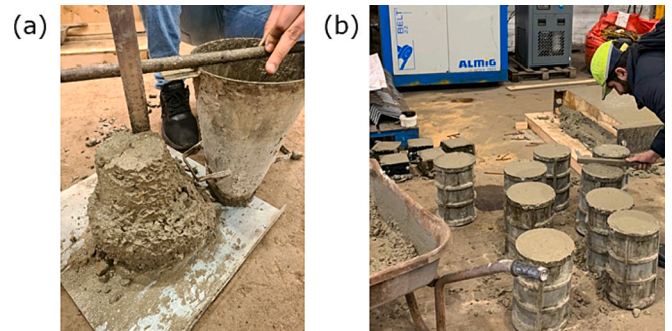


Fig. 6. (a) Slump test (b) Prepared concrete cylinders and cubes.

and 1560 kg/m<sup>3</sup> respectively. Standard tests were carried out to determine the properties of all materials (concrete and steel). The material properties of concrete obtained from compression and splitting tensile tests performed on the cylinders and cubes samples on the day of experiments in accordance with BS EN 12390-3 [29] and BS EN 12390-6 [30] are presented in Table 2. The average tensile strength of steel coupons obtained from shear connectors and steel beam section according to ISO 6892-1 [31] are presented in Table 3. Slabs were kept at the worksite for 30–50 days for curing at an average temperature of about 15 °C before moving them to the University of Leeds to prepare for testing.

**Table 2**  
Concrete properties on the day of the experiments.

Specimen	Concrete type	Average strength, (MPa)			E <sub>c</sub> (GPa)
		Cube - compressive	Cylinder - compressive	Split tensile	
NWC-230-SD	NWC	26.9	22.4	2.15	28.5
LWC-230-SD	LWC	26.2	21.56	1.86	11.05
LWC-230-D	LWC	26.4	22.46	1.97	11.7
NWC-300-SD	NWC	27.1	22.5	2.2	26.9

**Table 3**  
Mechanical properties of steel sections and shear connectors.

Coupons from	f <sub>y</sub> (MPa)	f <sub>u</sub> (MPa)	E <sub>s</sub> (GPa)
Webs of 230x75x26 PFC C-channel	434	545	200
Flanges of 230x75x26 PFC C-channel	405	528	200
Webs of 300x100x46 PFC C-channel	455	547	200
Flanges of 300x100x46 PFC C-channel	448	543	200
Web-Welded Shear Studs	450	530	200
Steel Dowels	320	450	200

**3.3. Test setup and loading protocol**

The four-point bending tests are carried out in accordance with the specifications of Eurocode 4 [27]. Test specimens are simply supported near the two ends of their lengths with an overhang of 100 mm at both ends. Two concentrated line loads of equal magnitudes are applied symmetrically on the middle part of the specimens using a 1000kN hydraulic jack and spreader beams to translate the load from the hydraulic jack to the specimens. The distance between the centreline of the line loads is 1000 mm and it is the same for all the tests. A load cell is connected to the hydraulic jack to record the loading readings and the whole loading apparatus is attached to the reaction frame as shown in Fig. 7, Fig. 8 & Fig. 9.

The static displacement controlled monotonic loading is applied in cycles, starting by applying three pre-loading incremental loading cycles in the elastic loading range to break local bonds between concrete and steel as well as to establish the residual deflections and slips within the elastic region. Each of these cycles is followed by a release. Then, a fourth cycle is applied on specimens up to the ultimate capacity (maximum expansion of the hydraulic jack) as presented in Table 4. To properly evaluate the flexural behaviour of PUSS® in the post-elastic range, the 4-point bending tests are displacement controlled, with a

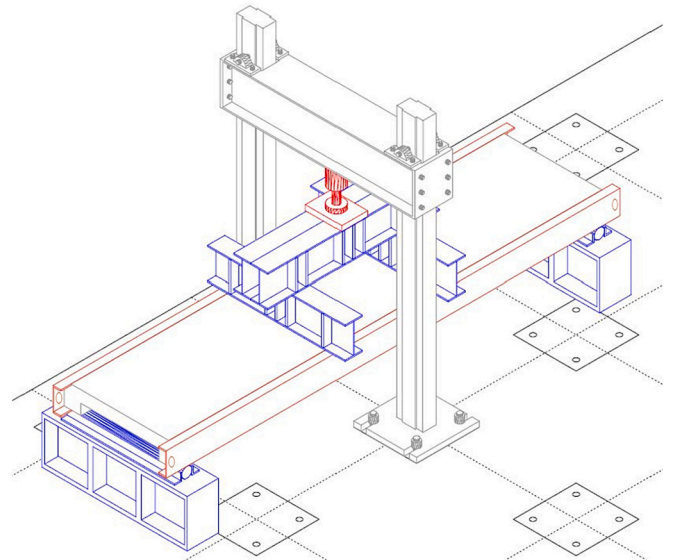


**Fig. 8.** 3D view sketch of the test setup for 4 m span PUSS® slab on the laboratory floor.

sufficiently small displacement rate (1 mm/min) to avoid dynamic impacts and to be able to track every damage in the specimens. Each test takes at least 3 h to conduct which is more than the minimum duration for the test specified by Eurocode 4 [27] stating that similar four-point bending tests on composite slabs should take at least 1 h before reaching failure.

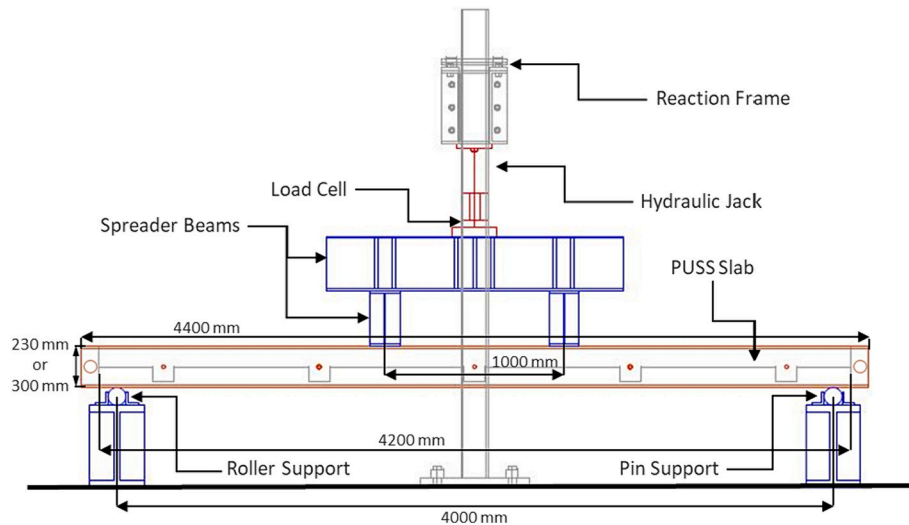


**Fig. 7.** Side view sketch of the test setup for 4 m span PUSS® slab.

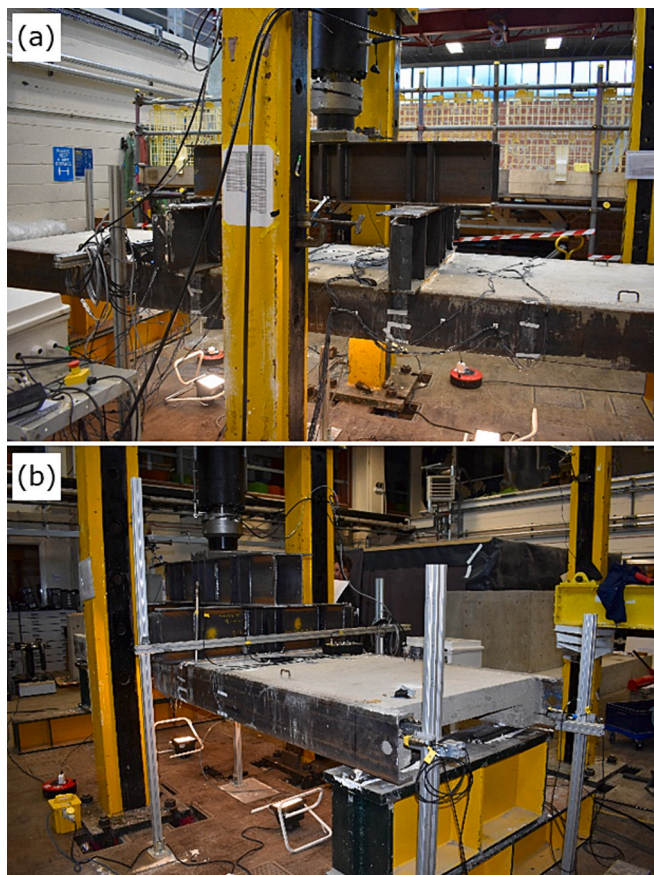


Fig. 9. Test setup.

Table 4  
Loading cycles.

Loading cycles	Aimed displacement	Displacement in mm
First cycle	1/3 x SLS max allowed deflection	≈ 4 mm
Second cycle	2/3 x SLS max allowed deflection	≈ 8 mm
Third cycle	1 x SLS max allowed deflection	≈ 12 mm
Final cycle	Maximum expansion of the hydraulic jack	≈ 170 mm

Maximum allowable SLS deflection =  $\text{span}/360 = 4000/360 = 11.11 \text{ mm}$

### 3.4. Instrumentation

A 1000kN hydraulic jack is used to apply the load (with a maximum extension of around 170 mm). A calibrated load cell is placed under the jack to measure the applied load, as shown in Fig. 7 to Fig. 9. To monitor the development of cracks with the increasing load/ deflection, a total of 8 cameras are distributed around the test setup to capture the cracks propagation on videos/ photos.

In addition, each specimen is calibrated to measure the strain, displacement and end-slip at various locations. Instruments such as strain gauges (singles and rosettes) as well as linear variable differential transformers (LVDT) are installed at multiple regions over the slabs. These regions are classified into 3 groups based on their distance from the mid-span of the slab, where region (I) stands for the strain gauges fixed at mid-span, while regions (II) and (III) are for strain gauges fixed at 0.5 m and 1 m distances from mid-span, respectively. The instruments are linked to a data logger (DAQ) system, which is connected to a computer to record all the readings at different load levels at once. The general instrumentation layout for the test setup is shown in Fig. 10. A total of twenty-three 5 mm strain gauges, seven 60 mm single strain gauges, four 5 mm rosettes and ten LVDTs are placed over each slab, taking into consideration the symmetry of the slab and loading frame.

## 4. Test results

The summary of the results obtained from the four 4-point bending tests on PUSS® units is presented in the following sections.

### 4.1. Maximum moment vs. mid-span deflection

The four experiments are ended upon the hydraulic jack extending to its maximum expansion (around 170 mm), while load plateauing is reached. At this point, none of the specimens shows complete collapse but multiple of the strain measurements in the steel exceeds the yielding point. In addition, several long deep cracks are detected at the bottom surface of the concrete slabs. At tests termination, all specimens' mid-span deflections exceed 160 mm ( $L/25$  or higher), surpassing significantly the serviceability (SLS) limits. Consequently, specimens are considered to have failed in all practical purposes. From the data collected from the LVDT attached to the hydraulic jack and the load cell, the "Maximum Moment vs. Mid-span Deflection" curves are derived for each test specimen and presented in Fig. 11. In addition, Table 5 gives a comparison of the value of the load reached at specific deflections during the experiments.

Taking a close look at the first 3 loading cycles in (Fig. 11 (b)), three different initial stiffnesses are obtained as anticipated, with NWC-300-SD being the largest due to the larger steel section, NWC-230-SD in the middle, and both LWC-230-SD and LWC-230-D having the lowest because of lower modulus of elasticity of LWC in comparison to NWC. It is worth noting that the latter two specimens have the same initial stiffness as they are made of the same steel C-channel section and concrete material, even though that different shear connectors are employed. This shows that the initial stiffness of PUSS® specimens is not influenced by the type/amount of shear connectors employed in the slabs, however, it is a function of the size of the steel section as well as the concrete strength and material. The figure also displays the effectiveness of the first three preloading cycles of all four tests in maintaining the same stiffness after each cycle and breaking the local bonds between steel and concrete. By having an overall view of the whole tests (Fig. 11 (a)), it is noticed that other than the initial stiffness, all four specimens show similar behaviours during the tests except NWC-300-SD reaching much higher capacity due to its deeper PFC C-channel sections. Furthermore, it is observed that the transition from the elastic region to yielding for both NWC specimens is steeper in comparison to LWC specimens. After yielding, all specimens start to gain a small additional capacity up to reaching the plateau. At the early plateau stage, they behave in an identical manner with NWC specimens having smoother lines until larger cracks and shear connectors failure start to appear causing some drops in the curves, which is discussed in more details in sections 4.4 and 4.5.

By comparing the maximum loads reached in each specimen from Fig. 11 (a) and Table 5, it is clear that the LWC-230-SD specimen gained a slightly higher maximum load in comparison to the NWC-230-SD specimen, although both have concretes of similar strengths. However, the use of lighter concrete in LWC-230-SD specimen reduces the dead load of the slab and allows it to gain capacity for higher live loads. On the other hand, LWC-230-D specimen showed lower capacity in comparison to the aforementioned specimens as the shear connectors used, which are composed of 3 steel dowels only, provide a lower degree of shear connection.

Finally, comparing the maximum moment capacities ( $M_{\text{Test}}$ ) obtained from the tests to the calculated maximum moment capacities using the stress block method ( $M_C$ ), a difference between 6.3% and 9.5% is recorded (Table 6). This can be attributed to workmanship issues during the casting of the specimens outside controlled laboratory conditions. This indicates that the stress block method is accurate enough (<10% difference) to be used in predicting the moment capacity of PUSS® units. For a more precise prediction of the degree of shear connection in the LWC-230-D specimen, LWC-230-SD specimen is taken

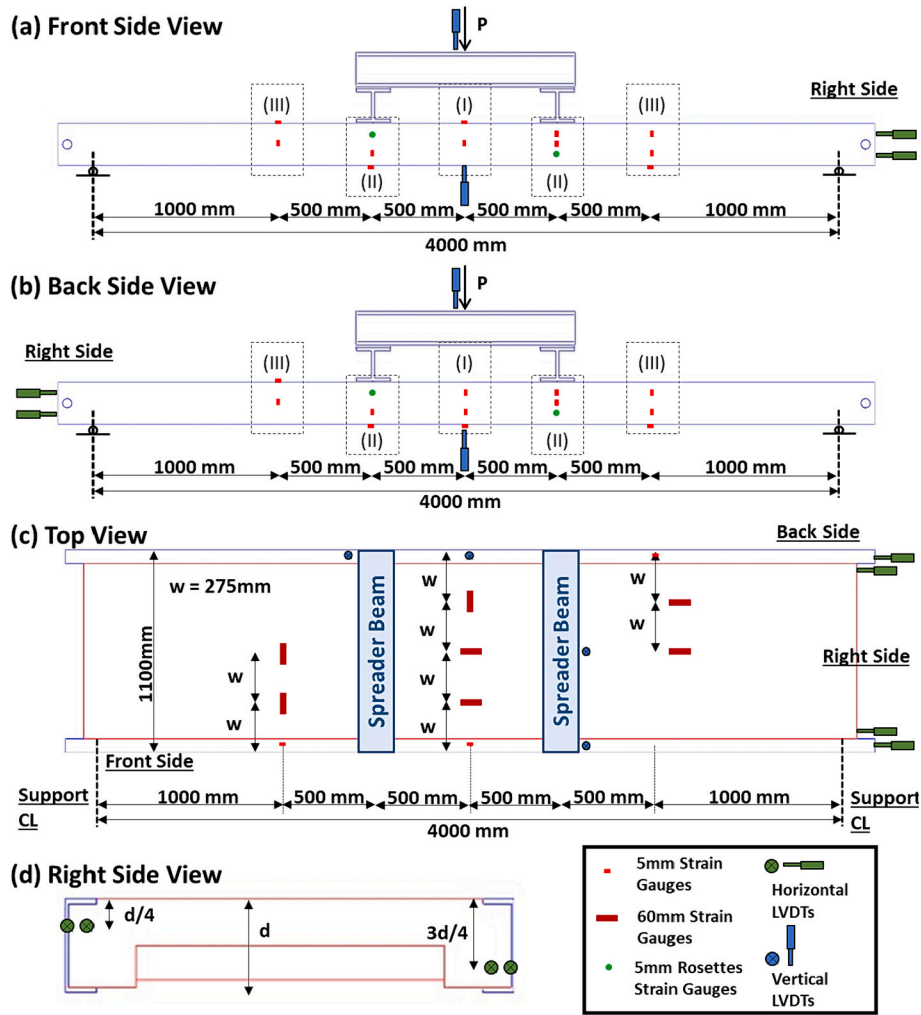


Fig. 10. Strain gauges, rosettes strain gauges and LVDTs layout.

as a reference and its test moment capacity is considered in Table 6 to be equal to the calculated moment capacity of LWC-230-D at full degree of shear connection. This makes the difference between the test's maximum moment capacity ( $M_{Test}$ ) and the calculated maximum moment capacity ( $M_{C2}$ ) for LWC-230-D equal to 1.7% which is fairly low. It is worth mentioning that when EC4, ANSI/AISC 360–10 and AASHTO [23–25] (Eqs. 2 to 4) employed to evaluate the degree of shear connection for LWC-230-D and NWC-300-SD, the calculated results did not match well the experimental results. The calculated values show that the LWC-230-D specimen exhibits degree of shear connection between 90% and 100% while for the NWC-300-D specimen exhibits degree of shear connection of 100%. The moment capacities obtained from the tests ( $M_{Test}$ ) as shown in Table 6 for the two specimens, demonstrated that the moment capacities reached in the tests are closer to the calculated values of moment capacities ( $M_C$ ) at the degree of shear connections obtained from Eq. 1 [9], which proves that Eq. 1 is more accurate than the aforementioned equations (Eqs. 2 to 4) in estimating the shear resistance of the shear connectors  $P_{sd}$  in PUSS®. However, as this equation is derived barely on direct shear push-out test results, it can be improved by taking into consideration the results from this research which studies the performance of the shear connectors under flexural loading.

#### 4.2. Stress distribution in steel sections

Fig. 12 displays the recorded strains measured in the PFC C-channel sections at various stages of the tests and at multiple distances from slabs' mid-spans (locations I, II and III in Fig. 10 (a)). The strain gauges at these locations are placed at the top and bottom flanges as well as three strain gauges along the height of the webs to capture the stress distribution along the height of the steel sections. The presented strain readings are from the stages of (1) the mid-elastic region, (2) the beginning of the plateau, and (3) the mid-plateau of each specimen. Note that each specimen has strain gauges placed at multiple symmetric spots to account for the unlike event of having some damaged gauges; hence, some of the readings presented in the figure are averaged from more than one reading and some are for one reading only. In addition, as it was not possible to attach strain gauges on the top flanges at location II (directly below the load spreader beams), the provided strains in the figure at these locations are estimated by assuming a linear variation of strains through the steel section.

By taking an overall look at the figure, it is observed that the steel sections of all specimens have similar strain development during the test. General similarities and differences that can be derived from the figures are summarised below:

- 1) In all the locations of all specimens, the strains in the top flanges (which are in compression) are always lower than the strains in the

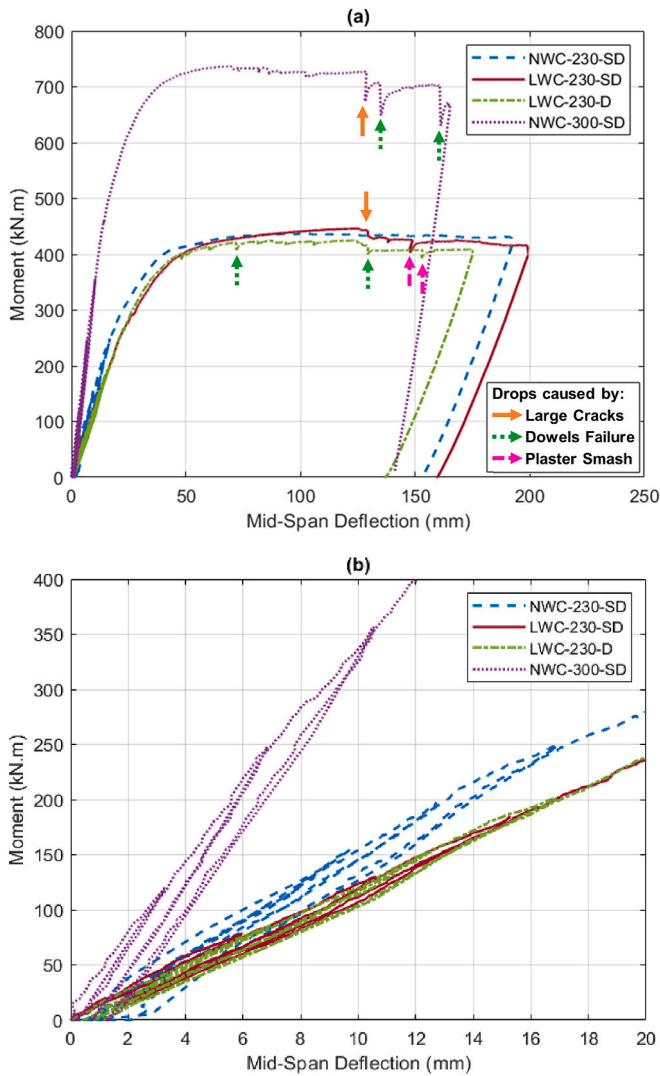


Fig. 11. Relationship between moment and mid-span deflections (a) for the whole tests (b) for the first three pre-loading cycles.

Table 5  
Comparison of load values at specific stages of the tests.

Mid-span displacement (mm)	Load (kN) in specimen			
	NWC-230-SD	LWC-230-SD	LWC-230-D	NWC-300-SD
4 mm of first loading cycle	119.4	77.7	67.4	192.1
8 mm of second loading cycle	216.5	130.3	129.2	377.8
12 mm of third loading cycle	296.5	196.7	192.1	531.3
20 mm of the final cycle	414.0	315.0	318.2	735.0
40 mm of the final cycle	551.0	495.0	504.0	941.6
Maximum load (kN)	582.9	594.9	566.4	982.2
Moment at maximum load, i.e. moment capacity (kN.m)	437.2	446.2	424.8	736.6

bottom flanges (in tension), meaning the P.N.A. of the sections is above the mid-height of the sections. Therefore, more focus is on the bottom strains in the following points. In addition, near linear variation of stresses over the cross-section can be captured.

2) Location III (1 m from the mid-span) has the lowest strains development at different stages of the tests as it is far from the maximum moment area (between the loading points), where the maximum strain in the bottom flanges at the mid-plateau stage barely reaches

Table 6  
Evaluation of test results in comparison to calculated capacities using stress block method.

	NWC-230-SD	LWC-230-SD	LWC-230-D	NWC-300-SD
Calculated moment capacity of steel section, $M_s$ (kN.m)	304.9	304.9	304.9	678.4
Calculated moment capacity of composite section at full degree of shear connection, $M_{C,Full}$ (kN.m)	409.3	408.7	408.7	837.5
Calculated degree of shear connection ( $\eta$ )	100%	100%	67%	57%
Calculated moment capacity of composite section at the degree of shear connection, $M_C$ (kN.m)	409.3	408.7	399.7	814.0
Test moment capacity, $M_{Test}$ (kN.m)	437.2	446.2	424.8	736.6
$M_{Test}/M_C$	1.068	1.092	1.063	0.905
Modified moment capacity of composite section at full degree of shear connection based on test results, $M_{C,Test,Full}$ (kN.m)			446.2	-
Re-calculated degree of shear connection ( $\eta$ )			63%	-
Re-calculated moment capacity of composite section at the degree of shear connection, $M_{C2}$ (kN.m)			432.2	-
$M_{Test}/M_{C2}$			0.983	-

the yield strain (about  $2100 \mu\epsilon$ ) with the exception for LWC-230-SD where the yield strain is not reached.

- At location I (at mid-span), for the full shear connection specimens, i.e., NWC-230-SD and LWC-230-SD, the strains in the bottom flanges at the mid-elastic region are very close to the yield strain and this strain is exceeded in the start of the plateau region. On the other hand, for the other two specimens that have a lower degree of shear connection, lower strains are measured at the bottom flanges at these stages, just crossing the yield strain lines at the start of the plateau region.
- For location II (below the point loads), the case is a slightly different as all the specimens have almost similar values of strains at mid-span and at the start of the plateau regions; being around the yield strain at the first stage and almost doubling this value of strain at the second stage.
- At the third stage (mid-plateau), strains significantly increase in all the specimens, especially at the bottom flanges achieving over  $10,000 \mu\epsilon$  at locations I and II, that indicates reaching maximum capacities at these locations and leaving permanent deformations in the steel beams. The measured strains at these two locations are close to each other, which is mainly due to the constant moment between the two loading points. It can also be captured that at this stage and these locations, the stress variation along the depth of the steel sections is less linear. This is due to the high compression and tension stresses developed at the top and bottom flanges respectively because of bending after reaching the maximum capacities.
- In all specimens, it is evident from the figures that the depth of the neutral axis exhibits slight variations across different locations within the same specimen. This phenomenon can be attributed to the upward shifting of the neutral axis positions as the tension steel begins to yield and concrete initiates cracking. Consequently, it is observed that, typically, locations closer to the mid-span where bending moments are higher, demonstrate elevated neutral axes compared to locations farther from mid-span (location III).

As one might expect, at the final stages of loading, where ultimate capacities are reached, the PFC C-channels should undergo web crippling under the high concentrated loads. However, this was not the case when testing the PUSS® units, as the concrete partial encasement within the steel sections along the flanges and with shear connectors that prevent the steel sections from moving away from concrete, no obvious web crippling is noticed at any location along the steel sections.

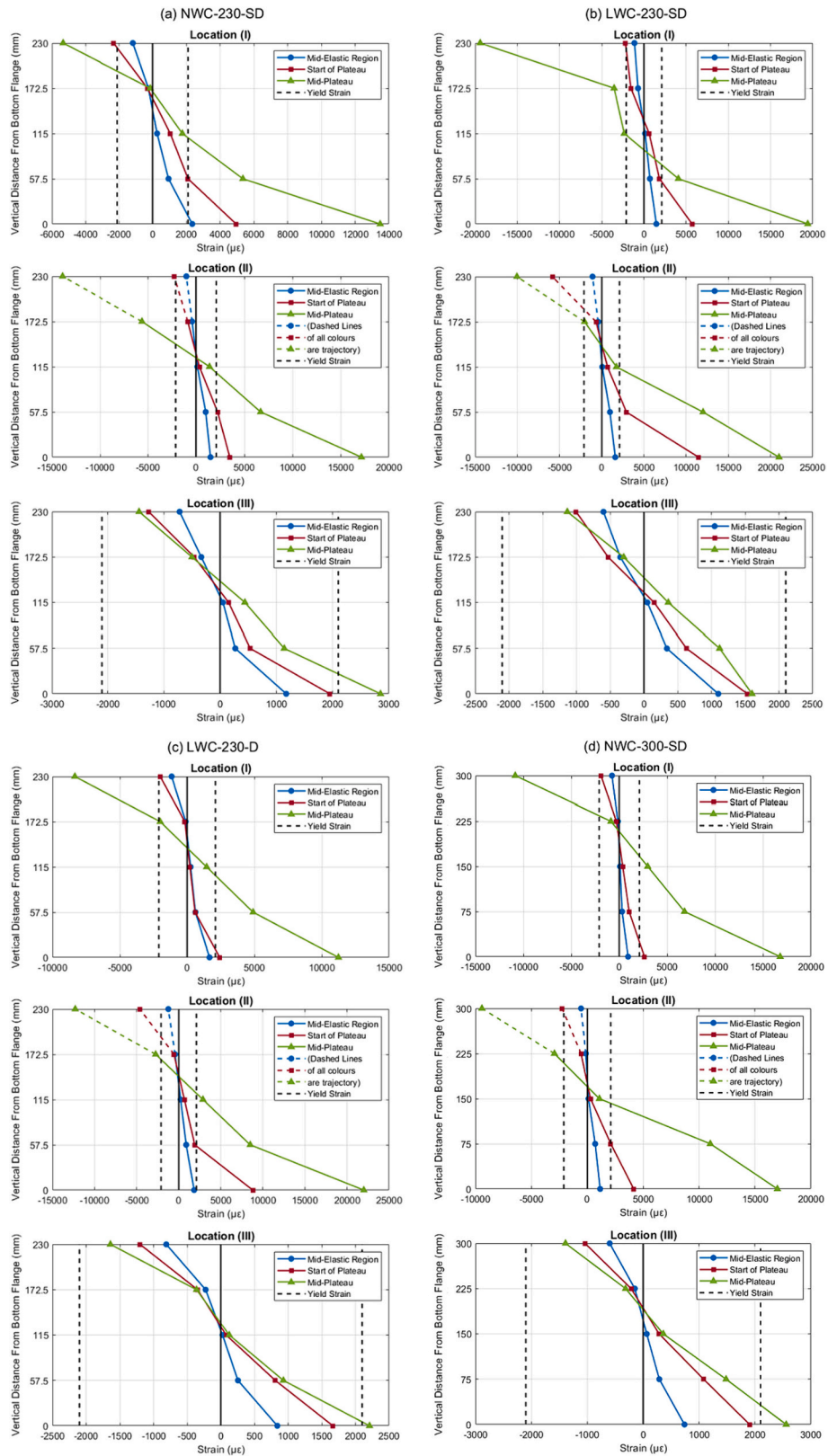


Fig. 12. Strains measured in steel section at different locations and different stages of tests.

### 4.3. Stress in concrete top surface

Capturing stress development in concrete is more challenging in comparison to steel sections, as cracks developing right underneath the attached strain gauges can jeopardise the readings, making it difficult to

record strains at the bottom surface of concrete. To obtain an overview of the strain/stress development at the top surface of concrete, the relationship between the hydraulic jack opening and the longitudinal strains measured at the top surface of concrete along the centreline of the slabs is captured herein and presented in Fig. 13. Fig. 13 (a) depicts strains

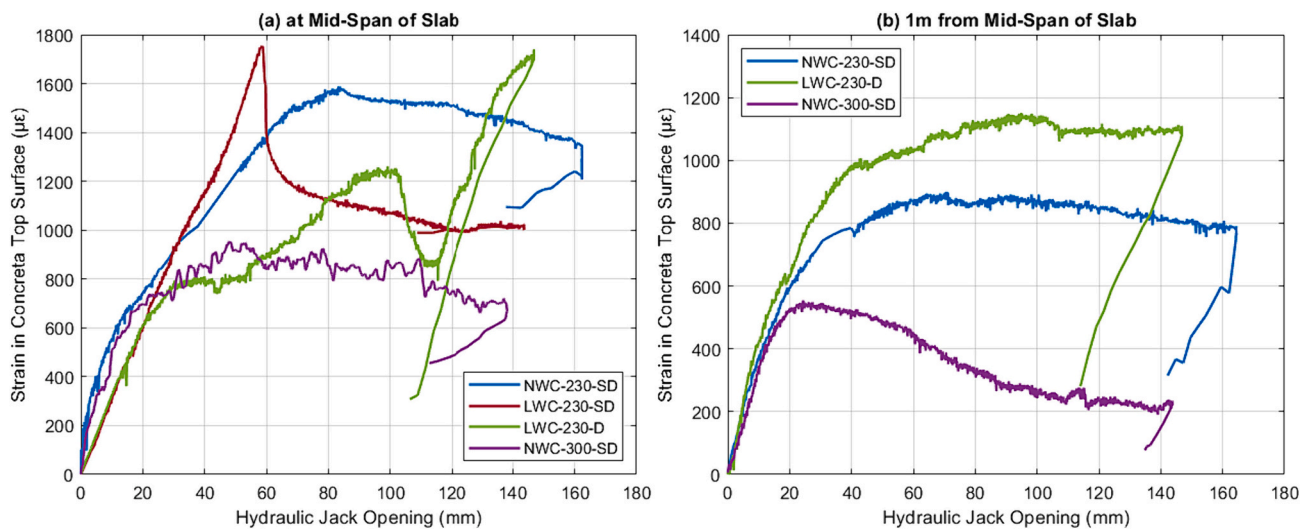


Fig. 13. Strains measured along the CL of the top surface of concrete at (a) mid-span (b) 1 m from mid-span.

recorded at the mid-span of the slab and Fig. 13 (b) depicts strains recorded at 1 m from the mid-span of the slab. Note that the strain gauge readings for the second location of LWC-230-SD are lost during the test and therefore not included in the figure.

From the two figures, some general outcomes can be concluded, as follows:

- 1) Moving farther from the mid-span reduces the measured strains (i.e., stresses) at the top surface of concrete because the applied moment becomes lower.
- 2) Test specimens with NWC have slightly higher stiffness at mid-span in comparison to specimens with LWC. This difference in stiffness is not very clear at 1 m distance from mid-span, which can be attributed to lower stress development at this location.
- 3) Because of the lower modulus of elasticity of LWC, similar stresses in LWC and NWC specimens result in higher strains in LWC in comparison to NWC. Therefore, the recorded strains in LWC specimens reach higher values during the tests in comparison to specimens with NWC. For example, specimens NWC-230-SD and LWC-230-SD are of comparable capacities and similar values of stresses are expected to be achieved at the concrete's top surface, which translates to higher strains in the LWC specimen.
- 4) By comparing the specimens of similar concrete materials (i.e., NWC-230-SD with NWC-300-SD and LWC-230-SD with LWC-230-D), it is observed that specimens with a lower degree of shear connection (LWC-230-D and NWC-300-SD) experience lower maximum strains developed in the concrete surface. This proves that the full capacity of concrete is not being utilised, as the shear connectors are not fully engaged and do not provide a full degree of shear connection. Moreover, it is noticed that at NWC-300-SD specimen (the one with the lowest degree of shear connection), at 1 m from the mid-span, the strains in the concrete started to decrease gradually after a 20 mm hydraulic jack opening, which is around the mid-elastic region. This shows that for specimens with lower degree of shear connection, at low moments locations, loads are mainly carried by steel sections with minimal contribution of the concrete.
- 5) The strain readings in LWC-230-SD at mid-span were expected to be larger, but a sudden reduction in strain was recorded at 60 mm hydraulic jack opening, which can be related to the occurrence of a crack beneath the strain gauge. Similarly, there is a drop in the strain for LWC-230-D at around 100 mm hydraulic jack opening due to the failure of one of the shear connectors at this point. Afterwards, the strains gradually resume increasing, showing redistribution of the loads after the failure of the shear connector.

#### 4.4. Crack development and failure mechanism

The video cameras placed beneath the test specimens allowed tracking of the crack development at the bottom ribbed surface of the concrete slab. The point at which cracks started to appear varies from specimen to specimen, but the main similarity is that they start with a horizontal hairline crack directly below the two loading points. The videos captured earlier development of visible cracks connected to the two sides of the slabs at lower loads in LWC specimens. For specimen NWC-230-SD, the horizontal hairline crack appeared during the final cycle at hydraulic jack opening equal to 6 mm and load to 138.3kN. This crack continued to grow until becoming more visible and connected to the two opposite steel sections at 25.7 mm hydraulic jack opening and load equal to 449.1kN. For specimen LWC-230-SD, the hairline crack onset appeared during the 2nd pre-loading cycle at hydraulic jack opening equal to 4 mm and load to 73.5kN. This crack continued to grow until becoming more visible and connected to the two opposite steel sections during the final cycle at 13.6 mm hydraulic jack opening and load equal to 253.8kN. For specimen LWC-230-D, the hairline crack started developing during the 3rd pre-loading cycle at hydraulic jack opening equal to 11.1 mm and load to 249.2kN. The crack continued to grow until becoming more visible and connected to the two opposite steel sections during the final cycle at 23.9 mm hydraulic jack opening and load equal to 413kN. For specimen NWC-300-SD, the hairline crack onset appeared during the 3rd pre-loading cycle at hydraulic jack opening equal to 10.2 mm and load to 396.7kN. This crack continued to grow until becoming more visible and connected to the two opposite steel sections during the final cycle at 16 mm hydraulic jack opening and load equal to 593.3kN. The order of load values at which cracks start to appear or spread between the opposite steel beams does not necessarily represent the order of strength of the specimens as several reasons cause some cracks to appear before others.

As the deflections increase, hairline cracks start to widen and grow gradually in depth. In addition, similar smaller cracks start to appear in the region around the previously developed cracks, having similar horizontal directions. At the end of the tests, a single clear deep horizontal crack surrounded by some smaller cracks is noticed below the loading points in NWC specimens. On the other hand, LWC specimens show more cracks forming a nest of deep horizontal cracks below the loading points. Fig. 14 captures the cracks below the loading points at the end of each test. Having a close look, it is observed that the cracks below the two loading points of each specimen are not of equal sizes as they differ in thickness by 2 to 4 mm. However, this difference is not of high significance as it is mainly caused by the smashing of the plaster

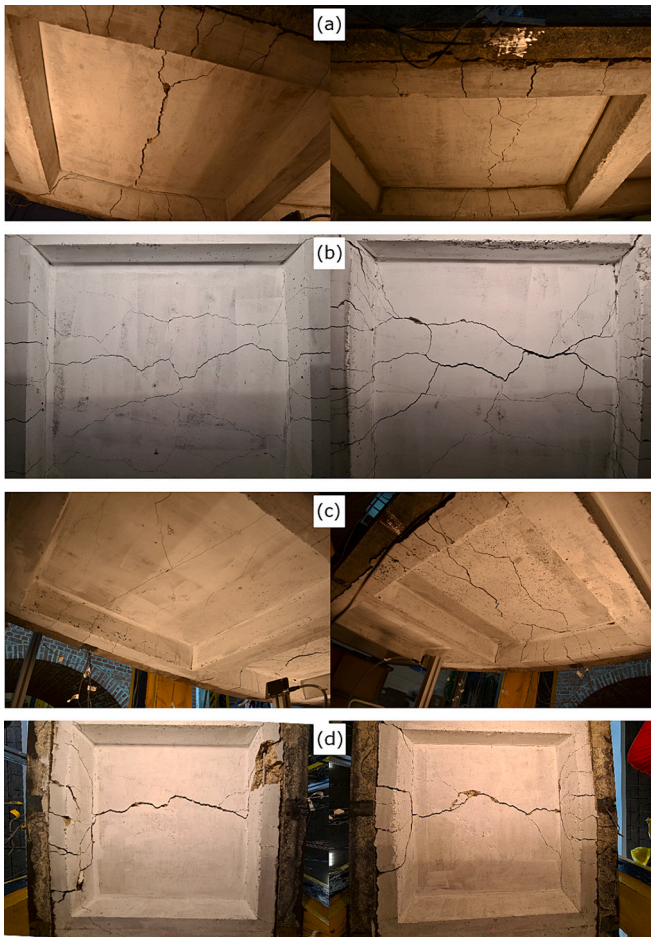


Fig. 14. Horizontal cracks at the end of the tests below loading points in (a) NWC-230-SD, (b) LWC-230-SD, (c) LWC-230-D and (d) NWC-300-SD.

below the spreader beams at some stage of the experiment causing a little movement of the beams and therefore, unsymmetrical load distribution. The horizontal cracks at the end of the tests indicate flexural failure of all specimens without signs of diagonal cracks that point out the presence shear failure.

The larger development of cracks in the LWC specimens is expected because of the lower stiffness of LWC in comparison to NWC specimens. However, this appears to have no effect on the capacity of the LWC specimens. The fact that they have similar strengths resulted in LWC-230-SD achieving even higher load capacity than NWC-230-SD. However, the larger number of cracks in the LWC specimens explains the greater number of reading-drops for the LWC specimens in the mid-span deflection versus moment curves, in the plateau region as shown in (Fig. 11 (a)). For every specimen, each new deep crack that started to appear caused a small drop in the curve followed by load redistribution causing the load to go back to its previous values. However, some large cracks resulted in loss of capacity, and thus permanent drop – such as the ones caused by large cracks developing in LWC-230-SD and NWC-300-SD at mid-span deflection  $\approx 125$  mm (see Fig. 11 (a)). In addition, there are drops caused by the failure of some of the shear connectors, as discussed in section 4.5.

#### 4.5. Shear connectors failure

A low degree of shear connection is applied in some specimens to study the failure of the shear connectors in PUSS® under flexural loading. As anticipated, failure of shear connectors was recorded for the specimens LWC-230-D and NWC-300-SD as they are designed with  $\eta$

values of 67% and 57%, respectively. The longitudinal shear causing failure of the shear connectors is larger near the supports and therefore, the failure of shear connectors in both specimens occurred at the shear connectors near the supports, which are the horizontal steel dowels. Every steel dowel is welded to the two opposite PFC C-channels, so when the bond (weld) on one side fails, it is considered that the steel dowel failed in shear. Another failure can possibly occur afterwards when the other side fails too.

For the LWC-230-D specimen, the first failure of one side of a steel dowel near the support occurred at mid-span deflection equal to 72 mm. A second failure also occurred at mid-span deflection around 125 mm but this time in the steel dowel near the other support. Both failures occurred in the connectors at the same side steel section. From Fig. 11 (a) in section 4.1, it is noticed that the first failure caused a little drop in the mid-span deflection versus moment curve, but the specimen regained its capacity after that, which indicates that the steel dowel is still active as it is still connected to the opposite steel section. On the other hand, the reading-drop associated with the second failure caused a permanent loss of capacity as one of the steel sections is no longer connected to the concrete slab (apart from one shear connector at mid-span which kept the steel section connected to the concrete but it does not contribute to the composite action), causing a reduction in the remaining degree of shear connection.

Specimen NWC-300-SD also experienced two shear failures in its shear connectors. The first failure occurred at the steel dowel near one of the supports at mid-span deflection equal to 135 mm. The second failure occurred at the same steel dowel but on the opposite side connected to the PFC C-channel at mid-span deflection equal to 160 mm. Fig. 11 (a) shows that the specimen recovered its capacity after the first failure, which indicates that the steel dowel is still active as it is still connected to the other side steel section. On the other hand, the reading-drop associated with the second failure caused a permanent loss of capacity as the steel dowel is no longer engaged, causing a reduction in the remaining degree of shear connection.

To visually examine the deformed shape of the shear connectors after being tested, the concrete around the locations of the shear connectors was removed to expose the connectors as presented in Fig. 15. Fig. 16 shows the condition of the undamaged shear connectors from specimens NWC-230-SD and LWC-230-SD. The condition of both damaged and undamaged shear connectors for specimens LWC-230-D and NWC-300-SD are captured in Fig. 17 and Fig. 18, respectively. It is observed that none of the shear connectors show any permanent deformation at the end of the tests, even for those that failed. It appears that the failed shear connectors have broken welds without having shown any bending in the steel dowels. In addition, exposing the sides of concrete slabs near the

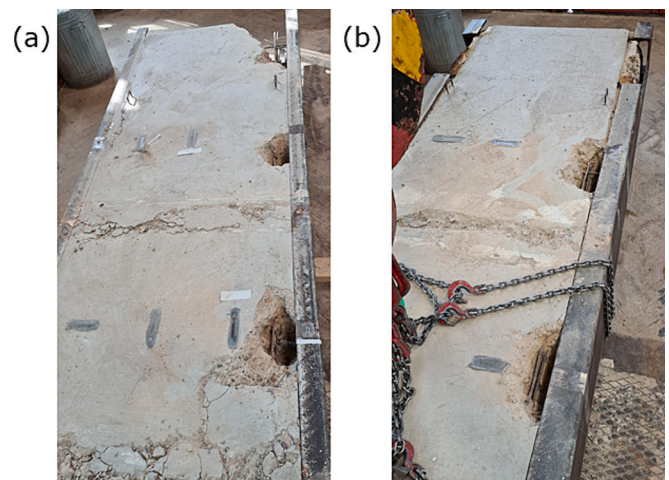


Fig. 15. Holes broken around shear connectors in specimens (a) NWC-230-SD and (b) NWC-300-SD.

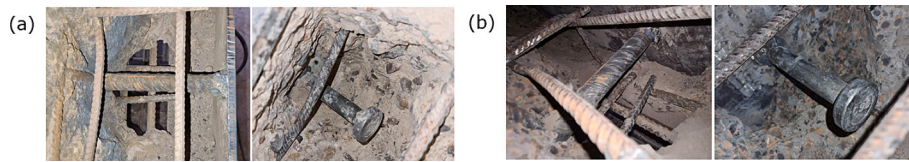


Fig. 16. Condition of shear connectors after the tests for (a) NWC-230-SD and (b) LWC-230-SD.

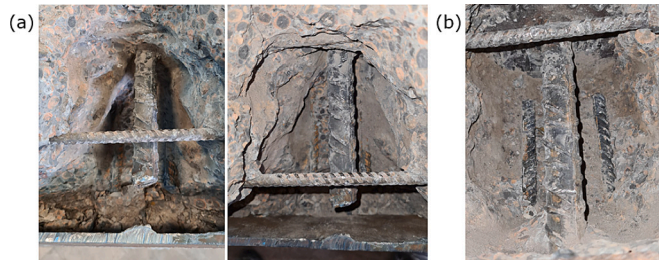


Fig. 17. Condition of (a) failed and (b) undamaged shear connectors after the test for LWC-230-D.

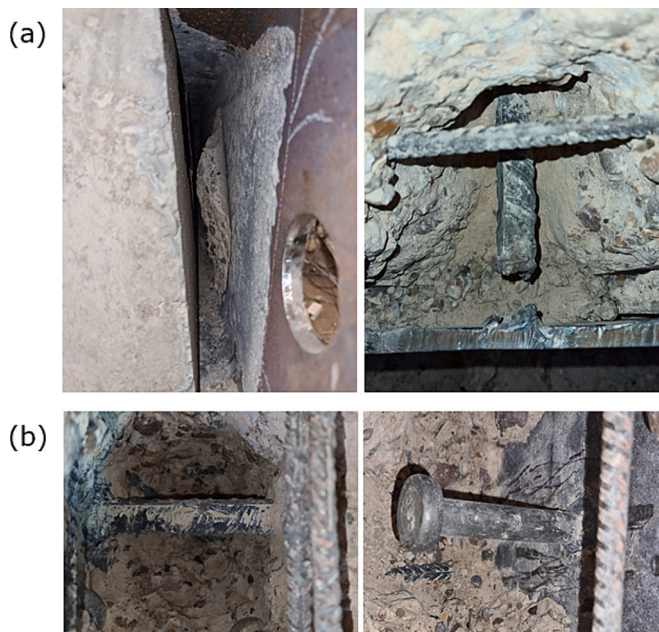


Fig. 18. Condition of (a) failed and (b) undamaged shear connectors after the test for NWC-300-SD.



Fig. 19. Cracks in concrete near the failed shear connectors in NWC-300-SD.

failed shear connectors by cutting steel edge beams in specimens LWC-230-D and NWC-300-SD revealed that some diagonal cracks started to develop near the shear connectors prior to their failure due to longitudinal and vertical shears as can be seen in Fig. 19.

#### 4.6. End-slip

Fig. 20 displays the relationship between the mid-span moment and end-slip between concrete and steel sections at the top and bottom flanges for each of the test specimens measured by the horizontal LVDTs placed at the ends of the slabs. It is shown that in the elastic region, none of the test specimens reached end-slips larger than 2 mm in the top or the bottom flanges. Thereafter, the end-slips increase rapidly during the plateau phase. The maximum end-slip at each flange of NWC-230-SD and LWC-230-SD specimens is between 3 mm to 5 mm. For specimens LWC-230-D and NWC-300-SD, similar end-slip behaviour as the aforementioned specimens is noticed before the failure of the first shear connector, reaching an average end-slips of 2 mm and 6 mm, respectively. However, following the failure of the shear connectors, end-slips values exhibited a precipitous escalation, reaching a maximum end-slips of 8 mm and 25 mm at the end of the tests, respectively. The much higher end-slip at the end of the test on NWC-300-SD is due to the higher depth as well as the failure of the steel dowel near the support where measurements are taken from both of its sides making complete separation between the concrete and steel sections. The shear connection system employed in PUSS® was tested previously to be ductile by Ahmed and Tsavdaridis [9] under direct shear tests, reaching end-slips at the failure of the shear connectors higher than the 6 mm which is the minimum value specified by Eurocode 4 [27] for ductile shear connector behaviour. Nevertheless, the distinct loading nature caused by bending on the shear connectors resulted in a different behaviour of the shear connectors, since the failed shear connectors did not experience any permanent deformation before their failure. In addition, end-slips higher than 6 mm is only reached after the failure of some of the shear connectors. These findings may not conclusively categorise the shear connectors of PUSS® as brittle in bending. It is important to note that the limits outlined in Eurocode 4 [27] for ductile behaviour of shear connectors mainly applicable for headed shear studs welded to the upper flange of composite beams. Consequently, there is a need for enhancements to account for horizontal shear connectors positioned at the mid-depth of composite sections.

More importantly, the results of bending tests demonstrate that PUSS® composite system as a whole behave in a ductile manner since the shear connection system in PUSS® units enable them to maintain structural integrity as unified rigid bodies without exhibiting any failure in the shear connectors until reaching ultimate load capacities of the slabs and high deflections exceeding at least four times of the SLS deflections. Furthermore, test results also evident that higher degree of shear connection result in achieving higher deflections before any shear connector failures occur.

Additional to end-slips, a horizontal separation between steel sections and concrete develops during the tests, especially at the end of the slabs. This separation was not monitored during the tests, but measured manually after the end of the tests. Fig. 21, Fig. 22 and Fig. 23 depict the separation at the end of the tests for all four specimens. The specimens that exhibited shear failure have much larger separation at locations near the failed shear connectors reaching values of 20 mm for the LWC-

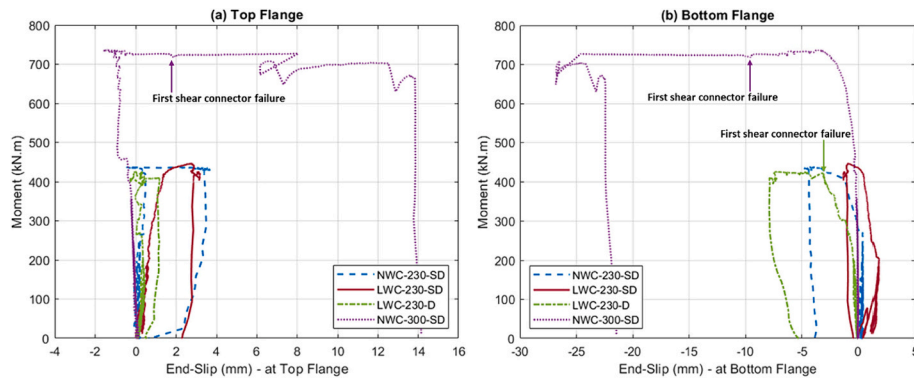


Fig. 20. Relationship between moment and end-slip at (a) top flange and (b) bottom flange.



Fig. 21. Separation between steel and concrete at the end of the tests for (a) NWC-230-SD and (b) LWC-230-SD.

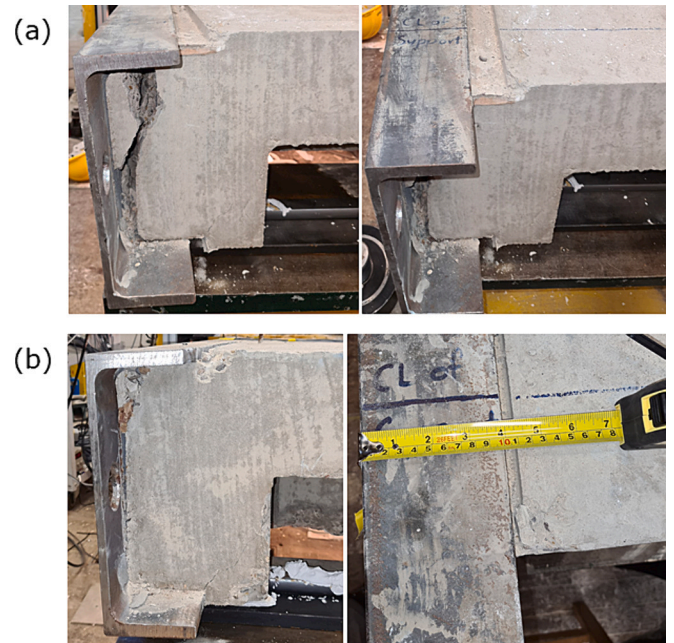


Fig. 23. Separation between steel and concrete at the end of the test for NWC-300-SD at the sides (a) near and (b) far from the failed shear connector.

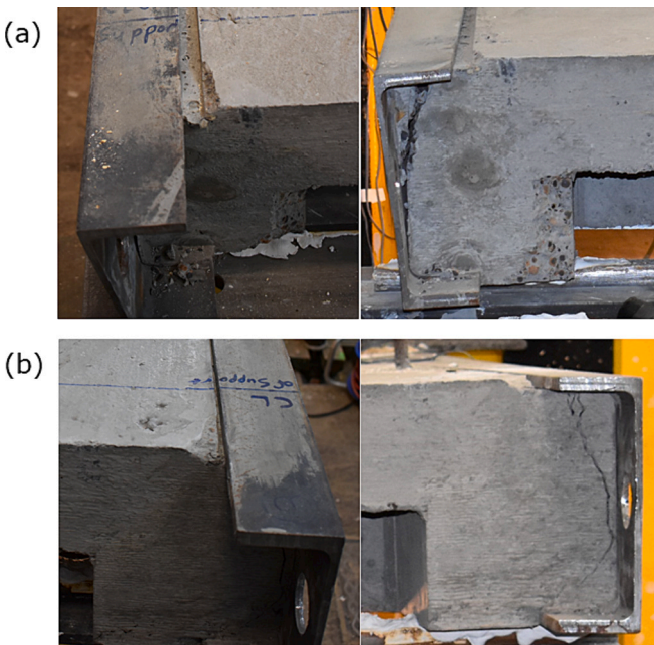


Fig. 22. Separation between steel and concrete at the end of the test for LWC-230-D at the sides (a) near and (b) far from the failed shear connector.

230-D specimen and 40-60 mm for the NWC-300-SD specimen. However, the maximum measured separation at the supports near the undamaged shear connectors in these two specimens as well as NWC-230-SD and LWC-230-SD is 5 mm.

### 5. Concluding remarks

This paper investigates the flexural behaviour of prefabricated steel-concrete composite ultra-shallow flooring units, aka PUSS®, by performing four full-scale 4-point bending tests, following push-out tests on the same system. Based on the results presented herein, the following points are concluded:

- PUSS® specimens made with LWC and NWC have similar performances in bending, and both can achieve similar moment capacities when NWC and LWC are made of similar concrete strengths. However, larger cracks develop during the tests on LWC specimens because of their lower modulus of elasticity. Test results showed that the development of these cracks causes an average of 7% loss of strength at later stages of the tests.
- PUSS® specimens with LWC demonstrate lower initial stiffness in bending in comparison to PUSS® specimens with NWC. However,

those with LWC can also accommodate slightly higher live loads in comparison to those with NWC because of lower weight, which reduces the dead load on slabs.

- Lowering the degree of shear connection reduces the moment capacities of PUSS® units and causes failure to some of the shear connectors at higher displacements. The failure of the shear connectors results in further loss of moment capacity and causes separation between the concrete and the side steel sections.
- PUSS® with full degree of shear connection reaches end-slips lower than 6 mm at the end of the tests. On the other hand, the use of a lower degree of shear connection increases the end-slips to values higher than 6 mm but only after the failure of some shear connectors. The 6 mm limit specified by EC4 [27] for ductile behaviour of shear connectors is not necessarily relevant to the welded horizontal shear connectors employed in PUSS®. Therefore, further experimental tests/ FEA models with various degrees of shear connections are required to evaluate the ductility of the shear connection system and the associated end-slips as well as making the required enhancements to EC4.
- Shear connection system employed in PUSS® allows the whole composite system to behave in a ductile manner as a single rigid body and enables it to achieve deflections extremely greater than SLS deflections before any failure in the shear connectors occur, which proves the effectiveness of the applied novel shear connection system.
- The use of this type of shear connection system composed of web-welded shear studs and horizontal steel dowels proved to be very effective in bending and have high resistance to the longitudinal shear between the steel sections and concrete. None of the shear connectors exhibited any permanent deformation at the end of the tests (even the ones that failed). Furthermore, calculations and test results showed that only a small number of shear connectors is required in PUSS® to reach the full degree of shear connection in comparison to other shear connection systems with vertical studs. However, even a smaller number of shear connectors need to be employed in PUSS® to lower the degree of shear connection and achieve ductile behaviour.
- The formula for calculating the shear resistance of shear connections that was previously introduced by Ahmed and Tsavdaridis [9] (Eq. 1), was employed by the authors of this paper to produce a improved version for calculating the degree of the shear resistance and to evaluate the moment capacities of PUSS® with the stress block method. The new formula proved to give satisfactory results within a 10% difference in comparison to test results. Hence, it is accurate enough to be used in designing PUSS® units of similar dimensions to the examined specimens.

#### CRedit authorship contribution statement

**Ahmed Abdulla Alali:** Writing – original draft, Visualization, Validation, Methodology, Formal analysis, Data curation. **Konstantinos Daniel Tsavdaridis:** Writing – review & editing, Validation, Supervision, Resources, Project administration, Methodology, Investigation, Funding acquisition, Data curation, Conceptualization.

#### Declaration of competing interest

The authors declare that they have no known competing financial interests or personal relationships that could have appeared to influence the work reported in this paper.

#### Data availability

Data will be made available on request.

#### Acknowledgements

The authors would like to acknowledge SC4 Ltd. for their kind contribution in preparing, casting and curing the test specimens as well as providing the space to store them. Additionally, the authors would like to thank the University of Bahrain for the PhD Scholarship.pae

#### References

- [1] I.M. Ahmed, K.D. Tsavdaridis, The evolution of composite flooring systems: applications, testing, modelling and eurocode design approaches, *J. Constr. Steel Res.* 155 (2019) 286–300, <https://doi.org/10.1016/j.jcsr.2019.01.007>.
- [2] K.D. Tsavdaridis, C. D’Mello, M. Hawes, Experimental study of ultra shallow floor beams with perforated steel sections, in: *Nordic Steel 09*, 2–4 September 2009, Malmö, Sweden. Nordic Steel, 2009, pp. 312–319.
- [3] O. Hechler, M. Braun, R. Obiala, U. Kuhlmann, F. Eggert, G. Hauf, CoSFB—Composite slim-floor beam: experimental test campaign and evaluation, in: *Composite Construction in Steel and Concrete VII*, 28–31 July 2013, Palm Cove, North Queensland, American Society of Civil Engineers, Australia, 2013.
- [4] M. Lawson, P. Beguin, R. Obiala, M. Braun, Slim-floor construction using hollow-core and composite decking systems, *Steel Const.* 8 (2) (2015) 85–89, <https://doi.org/10.1002/stco.201510018>.
- [5] S. Chen, T. Limazie, Composite slim floor beams with innovative shear connections, *Proc. Inst. Civil Eng. Struct. Build.* 171 (1) (2018) 29–37, <https://doi.org/10.1680/jstbu.16.00171>.
- [6] M.S. Majdub, S. Baharom, A.W. Al Zand, A.A. Mutalib, E. Hosseinpour, Innovation of shear connectors in slim floor beam construction, *J. Eng. Des.* 2022 (2022), <https://doi.org/10.1155/2022/2971811>.
- [7] T. Limazie, S. Chen, Effective shear connection for shallow cellular composite floor beams, *J. Constr. Steel Res.* 128 (2017) 772–788, <https://doi.org/10.1016/j.jcsr.2016.10.010>.
- [8] E. Hosseinpour, S. Baharom, W.H.W. Badaruzzaman, A.W. Al Zand, Push-out test on the web opening shear connector for a slim-floor steel beam: experimental and analytical study, *Eng. Struct.* 163 (2018) 137–152, <https://doi.org/10.1016/j.engstruct.2018.02.047>.
- [9] I.M. Ahmed, K.D. Tsavdaridis, Shear connection of prefabricated slabs with LWC - Part I: experimental and analytical studies, *J. Constr. Steel Res.* 169 (2020) p106016, <https://doi.org/10.1016/j.jcsr.2020.106016>.
- [10] G. Coldebella, F.P.V. Ferreira, S. De Nardin, Shear forces transfer in steel-concrete slim floor with circular web opening and PCHCS, in: *Structures Vol. 38*, Elsevier, 2022, April, pp. 1295–1307, <https://doi.org/10.1016/j.istruc.2022.02.066>.
- [11] S. Chen, T. Limazie, J. Tan, Flexural behavior of shallow cellular composite floor beams with innovative shear connections, *J. Constr. Steel Res.* 106 (2015) 329–346, <https://doi.org/10.1016/j.jcsr.2014.12.021>.
- [12] N. Baldassino, G. Roverso, G. Ranzi, R. Zandonini, Service and ultimate behaviour of slim floor beams: An experimental study, in: *Structures vol. 17*, Elsevier, 2019, February, pp. 74–86, <https://doi.org/10.1016/j.istruc.2018.10.001>.
- [13] T. Sheehan, X. Dai, J. Yang, K. Zhou, D. Lam, Flexural behaviour of composite slim floor beams, in: *Structures vol. 21*, Elsevier, 2019, October, pp. 22–32, <https://doi.org/10.1016/j.istruc.2019.06.021>.
- [14] X. Dai, D. Lam, T. Sheehan, J. Yang, K. Zhou, Effect of dowel shear connector on performance of slim-floor composite shear beams, *J. Constr. Steel Res.* 173 (2020) 106243, <https://doi.org/10.1016/j.jcsr.2020.106243>.
- [15] C. Meyer, The greening of the concrete industry, *J. Cement Concrete Compos.* 31 (8) (2009) 601–605, <https://doi.org/10.1016/j.cemconcomp.2008.12.010>.
- [16] Y.H. Dong, L. Jaillon, P. Chu, C.S. Poon, Comparing carbon emissions of precast and cast-in-situ construction methods – a case study of high-rise private building, *Constr. Build. Mater.* 99 (2015) 39–53, <https://doi.org/10.1016/j.conbuildmat.2015.08.145>.
- [17] L. Jaillon, C.S. Poon, Sustainable construction aspects of using prefabrication in dense urban environment: a Hong Kong case study, *J. Cons. Manag. Econ.* 26 (9) (2008) 953–966, <https://doi.org/10.1080/01446190802259043>.
- [18] BS EN 1992-1-1, Eurocode 2: Design of Concrete Structures, Part 1-1: General Rules and Rules for Buildings, European Committee for Standardization, Brussels, 2004.
- [19] W.I. Simms, A.F. Hughes, *Composite Design of Steel Framed Buildings*. SCI publication P359, The Steel Construction Institute, 2011.
- [20] I.M. Ahmed, Shear Connection of a Prefabricated Lightweight Steel-Concrete Composite Flooring System, The University of Leeds, Doctor of Philosophy thesis, 2019.
- [21] A.A. Alali, K.D. Tsavdaridis, Flexural behaviour of prefabricated ultra-shallow steel-concrete composite slabs, *ce/papers 4* (2–4) (2021) 787–794, <https://doi.org/10.1002/cepa.1362>.
- [22] I.M. Ahmed, K.D. Tsavdaridis, Life cycle assessment (LCA) and cost (LCC) studies of lightweight composite flooring systems, *J. Build. Eng.* 20 (2018) 624–633, <https://doi.org/10.1016/j.job.2018.09.013>.
- [23] BS EN 1994-2: Eurocode 4, Design of Composite Steel and Concrete Structures, Part 2: General Rules and Rules for Bridges, in: *European Committee for Standardization*, 2005.
- [24] ANSI/AISC, AISC 360-10: Specification for Structural Steel Buildings, American National Standards Institute, Chicago, 2010.
- [25] AASHTO, LRFD Bridge Design Specifications, 9<sup>th</sup> edn, AASHTO, Washington, DC, 2020.

- [26] ACI Committee, Building Code Requirements for Structural Concrete (ACI 318–08) and Commentary, American Concrete Institute, 2008.
- [27] BS EN 1994-1-1, Eurocode 4: Design of Composite Steel and Concrete Structures, Part 1–1: General Rules and Rules for Buildings, European Committee for Standardization, Brussels, 2004.
- [28] BS EN 197–1, Cement–Part 1: Composition, Specifications and Conformity Criteria for Common Cement, British Standard, 2011.
- [29] BS EN 12390–3, Testing hardened concrete–Part 3: Compressive strength of test specimens, British Standard, 2019.
- [30] BS EN 12390–6, Testing Hardened Concrete–Part 6: Tensile Splitting Strength of Test Specimens, British Standard, 2009.
- [31] ISO 6892-1, Metallic Materials–Tensile Testing–Part 1: Method of Test at Room Temperature, 2019.